Proceedings of the 30th International Cosmic Ray Conference
Rogelio Caballero, Juan Carlos D'Olivo,
Gustavo Medina-Tanco, José F. Valdés-Galicia (eds.)
Universidad Nacional Autonóma de México,
Mexico City, Mexico, 2009
Vol. 6, pages 21-33

30TH INTERNATIONAL COSMIC RAY CONFERENCE

Transition from Galactic to Extragalactic Cosmic Rays

VENYA BEREZINSKY
INFN, Laboratori Nazionali del Gran Sasso, I-67010 Assergi (AQ), Italy
venya.berezinsky@lngs.infn.it

Abstract. The transition from galactic to extragalactic cosmic rays is discussed. One of critical indications for transition is given by the Standard Model of Galactic cosmic rays, according to which the maximum energy of acceleration for iron nuclei is of order of $E_{\rm Fe}^{\rm max} \approx 1 \times 10^{17}$ eV. At $E > E_{\rm Fe}^{\rm max}$ the spectrum is predicted to be very steep and thus the Standard Model favours the transition at energy not much higher than $E_{\rm Fe}^{\rm max}$. As observations are concerned there are two signatures of transition: change of energy spectra and elongation rate (depth of shower maximum in the atmosphere $X_{\rm max}$ as function of energy). Three models of transition are discussed: dip-based model, mixed composition model and ankle model. In the latter model the transition occurs at the observed spectral feature, ankle, which starts at $E_a \approx 1 \times 10^{19}$ eV and is characterised by change of mass compostion from galactic iron to extragalactic protons. In the dip model the transition occures at the second knee observed at energy $(4-8) \times 10^{17}$ eV and is characterised by change of mass composition from galactic iron to extragalactic protons. The mixed composition model describes transition at $E \sim 3 \times 10^{18}$ eV with mass composition changing from galactic iron to extragactic mixed composition of different nuclei. These models are confronted with observational data on spectra and elongation rates from different experiments, including Auger.

Introduction

The Ultra High Energy Cosmic Ray (UHECR) has two most important problems. One of them is a presence of spectrum features produced by propagation of UHECR particles through Cosmic Microwave Radiation (CMB) and the second is transition from galactic to extragalactic Cosmic Rays (CR).

In the case of extragalactic protons two spectral signatures caused by interaction with CMB are predicted: Greisen-Zatsepin-Kuzmin (GZK) cutoff [1] and pair-production dip [2].

GZK cutoff is most spectacular prediction for UHECR, which status is still uncertain in present observations, though there are the indications to its presence.

The pair-production dip is the spectral feature originated due to electron-positron pair production by extragalactic protons interacting with CMB: $p + \gamma_{\rm CMB} \to p + e^+ + e^-$. Recently this feature has been studied in the works [3, 5, 4]. The dip has been observed with very good statistical significance χ^2/d.o.f.~ 1 by the Fly's Eye, Yakutsk, Akeno-AGASA and HiRes detectors, and with much worse statistical significance by Auger detector.

The pair-production dip and GZK cutoff are signatures of protons. The confirmation of the shape of these features is the evidence for proton-dominated composition of primary CRs. For nuclei as primaries the shape of the dip and GZK cutoff are strongly modified.

The different explanation of the dip has been proposed by Hill and Schramm [6]. They interpreted the dip observed in 1980s in terms of two-component model. The low energy component can be either galactic or produced by Local Supercluster. The similar model has been considered in [7]. The Hill-Schramm dip is widely used now for the explanation of the observed dip.

From 1970s in the UHECR spectrum there was observed a flattening, which is called *ankle*. Discovery of this feature at Haverah Park detector was interpreted as transition from the steep galactic component to more flat extragalactic one. The transition at ankle has been recently considered in [8].

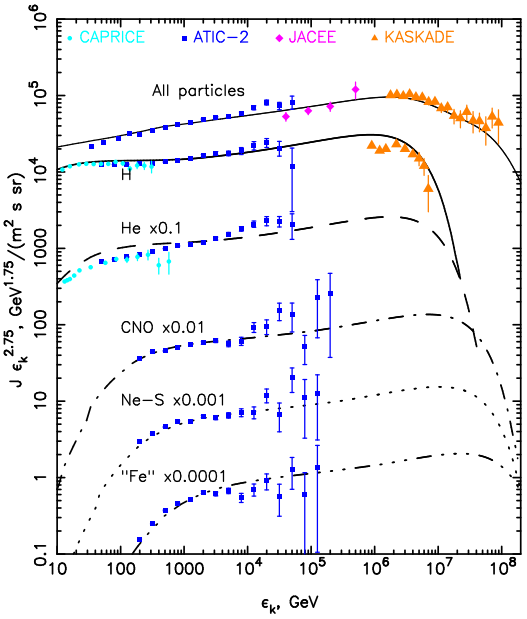

Fig. 1. Fluxes and spectra calculated within Standard Model in [21] for all particles, protons and nuclei are shown as function of kinetic energy ϵ_k. They are compared with data of CAPRICE, ATIC-2, JACEE and KASCADE. The position of the knees for all nuclei are given by $\epsilon_{\rm kn} \approx 3Z \times 10^{15}$ eV. The end of Galactic spectrum is given by iron knee $\epsilon_k \approx 8 \times 10^{16}$ eV. At higher energies galactic spectrum becomes very steep.

In the dip model the transition is completed at the beginning of the dip at $E \approx 1 \times 10^{18}$ eV. The ankle in this model appears as intrinsic part of the dip. Like in ankle model, the transition occurs here also as intersection of flat extragalactic component (this flatness is especially prominent in case of diffusive propagation) with steep galactic spectrum.

In the dip and ankle models the extragalactic component is assumed to be proton dominated, while the galactic component is most probably composed by iron nuclei. In the *intermediate model*, where transition occurs in the middle of the dip, the extragalactic CRs are assumed to have mixed composition [9].

In this paper all three above-mentioned models of transition are discussed. The logic of our discussion is as follows: we approach first the transition from the high energy end of galactic CRs, then we discuss the properties of UHECR relevant for transition problem and finally we describe the transition from properties of these two components.

The end of galactic CRs

With some disturbing small contradictions one may claim that at present we have the Standard Model for Galactic Cosmic Rays. It is based on Supernova Remnant (SNR) paradigm and includes four basic elements: (i) Supernova Remnants as the sources, (ii) SNR shock acceleration, (iii) Rigidity-dependent injection as mechanism providing the observed CR mass composition and (iv) Diffusive propagation of CRs in the galactic magnetic fields.

(i) SNRs are able to provide the observed CR energy production in Galaxy, which can be found as $Q \approx \omega_{\rm cr} c M_g / x_{\rm cr}$ [17], where $\omega \approx 0.5$ eV/cm^3 is the observed CR energy density, c is velocity of CR particle, $M_g \approx 5 \times 10^{42}$ g is the total mass of galactic gas, and $x_{\rm cr} \approx 7$ g/cm^2 is the grammage traversed by CR before escaping from Galaxy. Using these numbers one obtains $Q \approx 2 \times 10^{40}$ erg/s, which is less than 10% of energy release in the form of kinetic energy SNR ejecta per unit time.

(ii) The great progress has been reached during last decade in the theory of acceleration. The cosmic ray streaming instability strongly amplifies the magnetic field upstream creating highly turbulent field with strength up to $\delta B \sim B \sim 10^{-4}$ G [10] (for recent works see [11]). At each moment of the shock propagation only particles accelerated to maximum energy $E_{\rm max}$ can escape outside. $E_{\rm max}$ reaches the highest value at the beginning of the Sedov phase and then diminishes due to shock deceleration. The spectrum of escaping particles has a narrow peak at energy $E_{\rm max}(t)$ at each moment t, but the spectrum integrated over time has a classical E^{-2} shape with flattening at highest energies. This interesting result has been recently obtained by Ptuskin and Zirakashvili [12].

The maximum acceleration energy estimated in the Bohm regime of diffusion in the acceleration process is given by

$$E_{\rm max} = 4 \times 10^{15} Z \frac{B}{10^{-4}{\rm G}} \left(\frac{W_{51}}{n_g/{\rm cm}^3} \right)^{2/5} \ {\rm eV}, \quad (1)$$

where B is amplified magnetic field, W_{51} is the kinetic energy of the shell in units 10^{51} erg, n_g is

upstream density of the gas and Z is charge number of accelerated nuclei. Thus for the protons and iron nuclei the maximum energies are

$$\begin{aligned} E_p^{\max} &= 4\times 10^{15} B_{-4}\ \mathrm{eV}, \\ E_{\mathrm{Fe}}^{\max} &= 1\times 10^{17} B_{-4}\ \mathrm{eV}. \end{aligned} \quad (2)$$

$E_p^{\max}$ describes well the position of the proton knee and $E_{\mathrm{Fe}}^{\max}$ predicts the position of iron knee.

(iii) As the observations show, nuclei are systematically more abundant in cosmic rays in comparison with interstellar medium in the solar neighborhood [13, 14, 15]. The injection of particles in the regime of acceleration is responsible for it [13, 14, 15]. It can be illustrated by simple consideration [16].

A particle i from downstream ($i = A,\ p$) can cross the shock and thus to be injected in the regime of acceleration, if its Larmor radius $r_L(p) \geq d$, where d is the thickness of the shock front. Thus we readily obtain the relation between nuclei and proton injection momenta

$$p_{\mathrm{inj}}^A = ZeBd/c = Zp_{\mathrm{inj}}^p. \quad (3)$$

Eq. (3) results in $v_{\mathrm{inj}}^A < v_{\mathrm{inj}}^p$, which provides the higher injection rate of nuclei.

This conclusion can be reached also in more formal way. Consider flux of accelerated particles i $J_i(p) = K_i(p/p_{\mathrm{inj}}^i)^{-\gamma_g}$. Normalizing $J_i(p)$ by condition

$$\frac{4\pi}{c}\int_{p_{\mathrm{inj}}^i}^{\infty} J_i(p)dp = \eta_i n_i, \quad (4)$$

where n_i is the density of gas i and η_i is a fraction of this density injected into acceleration process, we obtain for the ratio of fluxes of nuclei and protons in CRs

$$\frac{J_A(p)}{J_p(p)} = Z^{\gamma_g - 1}\frac{\eta_A n_A}{\eta_p n_p}. \quad (5)$$

Thus, fraction of nuclei is enhanced by factor $Z\eta_A/\eta_p$. For numerical calculations of CR nuclei abundances see [13, 14, 15].

(iv) CRs propagate in Galaxy diffusively, scattering off small-scale magnetic turbulence described as superposition of MHD waves with different amplitudes and random phases. This process is considered (see e.g. [17]) in the resonance approximation, when the giro-frequency of a particle is equal to a wave frequency in the system at rest with a motion of a particle along the average magnetic field. The magnetic field is separated into average (constant) field $\vec{B}_0$ and fluctuating component $\vec{B}$. In [17] the parallel diffusion coefficient $D_{\parallel}(E)$ is calculated assuming $D_{\perp}(E)$ being much smaller than $D_{\parallel}(E)$ (see however the numerical simulations [18] which does not support this assumption for the highest energies).

The diffusion coefficient and its energy dependence is primarily determined by spectrum of turbulence $w(k)$ which in most important cases is given in the power-law form $w(E) \propto k^{-m}$, where k is a wave number. Then one has

$$w(k) \propto k^{-m},\ \ D(E) \propto E^{-n},\ \ n = 2 - m. \quad (6)$$

Thus, we obtain for the Kraichnan turbulence spectrum, which Landau and Lifshitz [19] consider theoretically preferable for MHD waves, $m = 3/2$ and $D(E) \propto E^{1/2}$; for the Kolmogorov spectrum $m = 5/3$ and $D(E) \propto E^{1/3}$ and for diffusion in shock-dominated turbulence $m = 2.0$ and $D(E) = const$. In the cases when the turbulent magnetic component δB is much larger than regular component B_0 the Bohm diffusion is valid $D(E) \propto E$; this case is in particular valid for acceleration on the shock fronts.

Diffusive propagation is the only phenomenon. which imposes currently the problems for the Standard Model of Galactic CRs. The essence of this problem can be easily seen.

Using the generation spectrum in the Galaxy, as that in acceleration $Q_{\mathrm{gen}}(E) \propto E^{-2}$, one obtains the diffuse spectrum:

$$J(E) \propto Q_{\mathrm{gen}}(E)/D(E) \propto E^{-(2+n)}. \quad (7)$$

Then from the observed spectrum $J(E) \propto E^{-2.7}$ one obtains $D(E) \propto E^{0.7}$, which in principle results in too high anisotropy $\delta(E) \propto D(E)$ and too low traversed grammage $x_{\mathrm{cr}}(E) \propto 1/D(E)$ at high energy E. There are suggestions how these problems may be solved: the problem of small $x_{\mathrm{cr}}(E)$ - by spallation inside CR sources and reacceleration, the problem of anisotropy - by local character of this phenomenon, and flat spectrum of helium - by acceleration in SNI remnant enriched

by helium (see [20, 21] for discussion and references).

The proton and nuclei spectra calculated recently by Berezhko and Völk [21] within Standard Model are shown in Fig. 1 in comparison with observational data. The agreement with observations is quite good at low energies, and the knee is confirmed at $E_{\rm kn} \approx 3 \times 10^{15}$ eV in proton and all-particle spectra. The iron knee located at $E_{\rm Fe} \approx 8 \times 10^{16}$ eV is most important prediction of Standard Model. The spectra beyond the knees are predicted to be very steep. additionally included

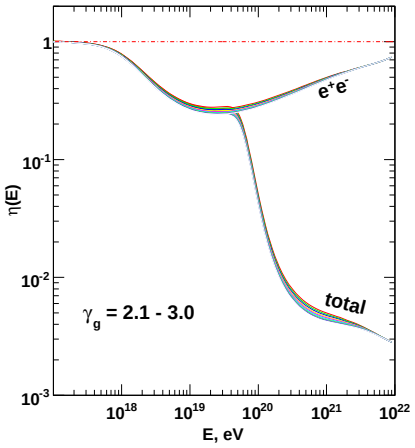

Fig. 2. Modification factor

one obtains dip, shown in Fig. 2 by curve "e^+e^-". If to include the pion production, the GZK feature appears (curve "total").

Pair-production dip and GZK cutoff

Being a quite faint feature, the e^+e^--production dip is not seen well in the naturally presented spectrum $\log J(E)$ vs. $\log E$. The dip is more pronounced when analyzed in terms of the *modification factor* [2, 3]. It is defined as a ratio of the spectrum $J_p(E)$ calculated with all energy losses taken into account , and unmodified spectrum $J_p^{\rm unm}(E)$, where only adiabatic energy losses are included.

$$\eta(E) = J_p(E)/J_p^{\rm unm}(E) \qquad (8)$$

The modification factor is presented in Fig. 2. If one includes only adiabatic energy losses, $\eta(E) = 1$ according to definition (dash-dot line). If e^+e^--production energy losses are

The observable part of the dip extends from beginning of GZK cutoff at $E \approx 4 \times 10^{19}$ eV down to $E \approx 1 \times 10^{18}$ eV, where $\eta \approx 1$. It has two flattenings: one at energy $E_a \approx 1 \times 10^{19}$ eV and the other at $E_b \approx 1 \times 10^{18}$ eV. The former automatically produces ankle (see Fig. 3) and the latter provides the intersection of flat extragalactic spectrum at $E \leq 1 \times 10^{18}$ eV with more steep galactic spectrum.

The modification factor is less model dependent physical quantity than the spectrum. In particular it depends weakly on spectral index of generation spectrum γ_g: In Fig. 2 the curves are plotted for $2.1 \leq \gamma_g \leq 3.0$ with intervals $\Delta\gamma_g = 0.1$. The remarkable property of visible dip in terms of modification factor is its *universality*. Modification factor $\eta(E)$ is given as dimensionless numbers for different energies and the curve remains the same when various physical phenomena are included in calculations [4]: discreteness in the source distribution (the distance between sources may change from 1 Mpc to 60 Mpc), different modes of propagation (from rectilinear to diffusive), local overdensity or deficit of the sources, large-scale inhomogeneities in distribution of sources, some regimes of cosmological source evolution (most notably those observed for AGN) and interaction fluctuations. The only phenomenon which modifies dip noticeably is presence of more than 15% of nuclei in primary radiation. Therefore the proton dip in terms of modification factor is the universal spectral feature, determined mostly by interaction with CMB.

The *observed* modification factor is given according to definition by the ratio of observed $J_{\rm obs}(E)$ to unmodified ($J_{\rm unm}(E) \propto E^{-\gamma_g}$) spectrum: $\eta_{\rm obs} \propto J_{\rm obs}(E)/E^{-\gamma_g}$, where γ_g is the exponent of the generation spectrum $Q_{\rm gen}(E_g) \propto E_g^{-\gamma_g}$ in terms of initial proton energies E_g. *As Fig. 3 shows the pair production dip and beginning of GZK cutoff up to energy* 1×10^{20} *eV is reliably confirmed by all experimental data including AGASA.* As to AGASA excess at $E > 1 \times 10^{20}$ eV it can be explained by some other reasons, e.g. at some conditions by statistical fluctuations seen in MC of the work [23].

The comparison of the predicted dip with observational data includes only two free parameters:

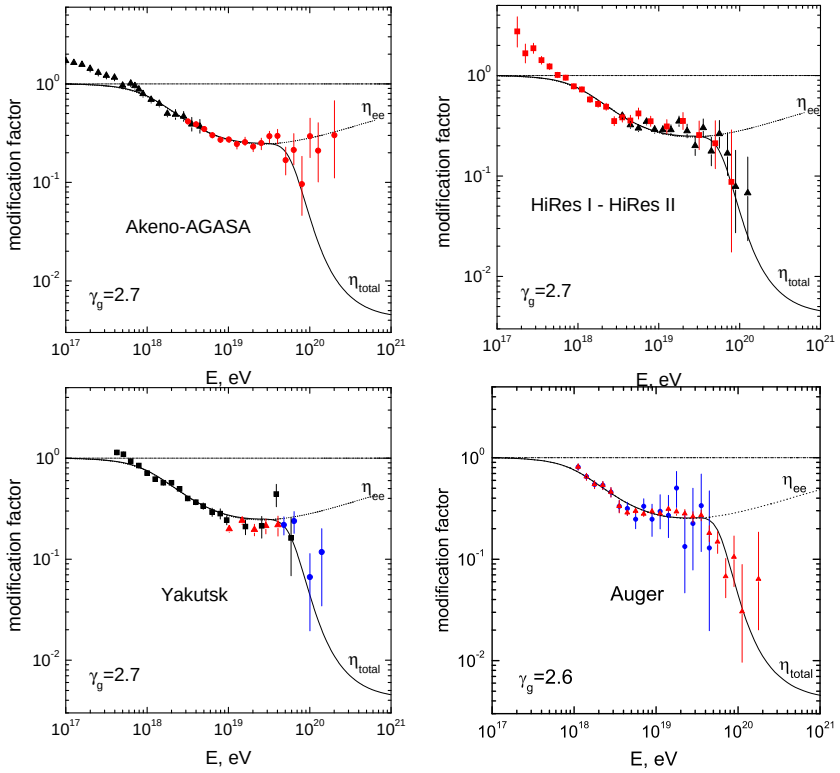

Fig. 3. The predicted pair-production dip in comparison with Akeno-AGASA, HiRes, Yakutsk and Auger data [22]. The first three experiments confirm dip with good $\chi^2/\mathrm{d.o.f.} \approx 1.0 - 1.2$, while the Auger data are characterized by larger $\chi^2/\mathrm{d.o.f.}$ (see the text).

exponent of the power-law generation spectrum γ_g (the best fit corresponds to $\gamma_g = 2.6 - 2.7$) and normalization constant to fit the e^+e^--production dip to the measured flux. The number of energy bins in the different experiments is 20 - 22. The fit is characterized by $\chi^2/\mathrm{d.o.f.} = 1.0 - 1.2$ for AGASA, HiRes and Yakutsk data. For the Auger data χ^2 is good for hybrid data and very bad for surface detector data, mainly due to data in two lowest energy bins at 4.3 and 5.5 EeV. In Fig. 3 the hybrid spectrum shown by circles, and combined spectrum (surface detector data combined with fluorescent data at low energies) shown by triangles are displayed. If to introduce the random energy errors $\delta E/E$ inside a bin (see section 'Discussion and Conclusions'), which is reasonable for the low energy end of the surface detector measurements, χ^2 is tremendously improved. The analysis will be presented somewhere else.

One can see that at $E < E_b = 1 \times 10^{18}$ eV the experimental modification factor, as measured by Akeno and HiRes, exceeds the theoretical modification factor. Since by definition modification factor must be less than one, this excess signals the appearance of a new component of cosmic rays at $E < E_b = 1 \times 10^{18}$ eV, and this component can be nothing but galactic cosmic rays. Thus, the transition from extragalactic to galactic cosmic rays, starts at energy E_b. The position and shape of the dip is robustly fixed by interaction with CMB and can be used for energy calibration of the detectors.

The systematic errors in energy measurements are high, from 15% in AGASA to 22% in Auger. To calibrate each detector we shift the energies by factor λ to reach minimum χ^2 in comparison with theoretical dip. We obtain these factors as $\lambda_A = 0.9$, $\lambda_{Ya} = 0.75$ and $\lambda_{Hi} = 1.2$ for AGASA, Yakutsk and HiRes detectors, respectively. After energy calibration the fluxes given by AGASA,

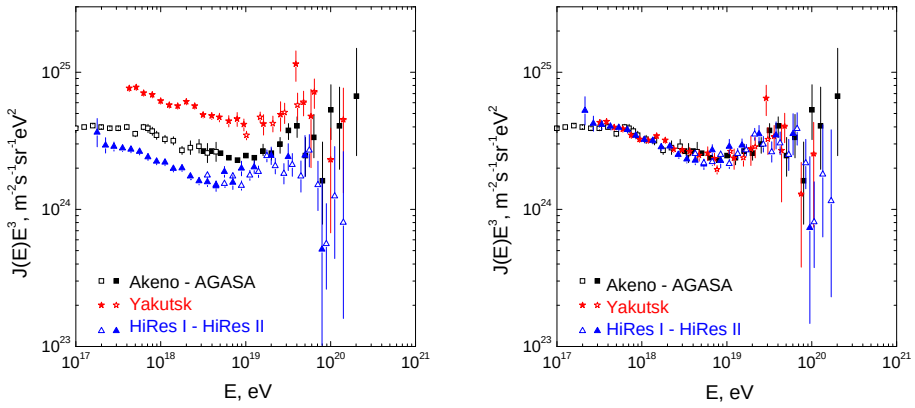

Fig. 4. The fluxes from Akeno-AGASA, HiRes and Yakutsk detectors before and after calibration.

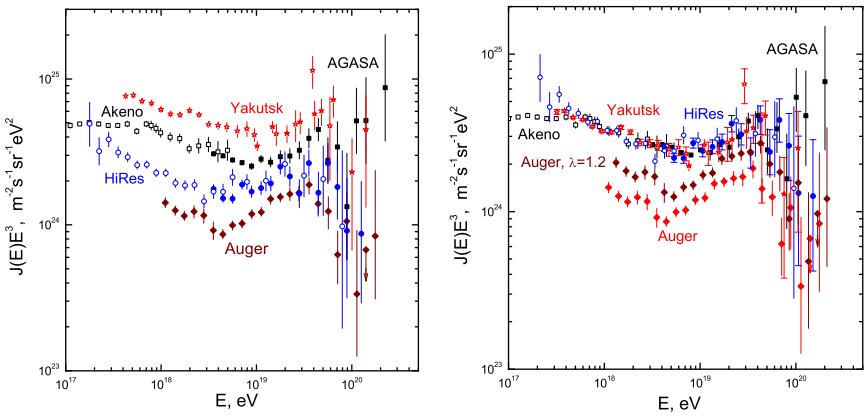

Fig. 5. Comparison of Auger data with AGASA, HiRes and Yakutsk (left panel) and comparison of Auger data and the energy shifted Auger data ($\lambda = 1.2$) with the dip-calibrated AGASA, HiRes and Yakutsk data (right panel).

HiRes and Yakutsk detectors agree with each other in a very precise way (see Fig. 4). The Auger flux is noticeably below the flux shown in Fig. 4.

In Fig. 5 we show in the left panel the comparison of Auger data with that of AGASA, HiRes and Yakutsk. In the right panel we compare the Auger flux with the calibrated data of AGASA, HiRes and Yakutsk. We use also the energy-shifted Auger data (curve $\lambda = 1.2$) with maximum shift allowed by systematic energy errors of Auger. One can see that disagreement in fluxes survives. M. Teshima in his rapporteur talk [24] noticed that shift with $\lambda \approx 1.5$ brings the data of Auger in agreement with the calibrated fluxes of AGASA, HiRes and Yakutsk.

Three models of the transition

In this section we describe three models of the transition from galactic to extragalactic CRs: *ankle*, *dip* and *mixed composition* models. One feature is common for all three models: they describe transition as intersection of steep galactic CR spectrum with more flat extragalactic spectrum. One criterion which all models should respect is agreement with the Standard Model of Galactic CRs. The observational data which has a power to confirm or reject each model include energy spectrum and mass composition.

Ankle model

This is a traditional model, based on the interpretation of the ankle as spectrum feature of the transition (see [8] for the recent works). In fact this is most natural model, where transition occurs because extragalactic component is very flat. This component is assumed to have pure proton composition with flat generation spectrum $\propto E^{-2}$ valid for non-relativistic shock acceleration. Energy losses modify spectrum insignificantly at $E \lesssim 4 \times 10^{19}$ eV. The beginning of the ankle $E_a \sim 1 \times 10^{19}$ eV corresponds to equal fluxes of galactic and extragalactic CRs at this energy. The transition at the ankle is illustrated by right panel in Fig. 6. The curve "extr.p" presents the calculated extragalactic flux of protons and the dash-dot line gives the galactic CR spectrum. It is obtained by subtracting the extragalactic flux from the total observed flux following the procedure first suggested in [25]. The observed dip in the spectrum is explained not by pair-production dip, but by Hill-Schramm mechanism [6]. One must assume that galactic flux is presented by iron nuclei, and even in this case the ankle model contradicts the Standard Model of Galactic CRs, since the half of the observed flux at $E \sim 1 \times 10^{19}$ eV has the galactic origin. This model needs another component of galactic CRs with acceleration to energy 100 times greater than maximum energy in the Standard Model.

Another problem of this model is given by measured *elongation rate* $X_{\max}(E)$, where $X_{\max}$ is the depth of the atmosphere (in g/cm^2) where a shower has maximum. In the right panel of Fig. 7 $X_{\max}(E)$ calculated for the ankle model is plotted in comparison with elongation rates measured by different detectors. One can see that in energy range $(1.5 - 5) \times 10^{18}$ eV there is great discrepancy between elongation rate calculated in all models with measurements of all detectors [26].

Dip model

It is based on spectral confirmation of *pair-production dip* in energy range $1 \times 10^{18} - 4 \times 10^{19}$ eV and beginning of GZK cutoff in energy range $4 \times 10^{19} - 1 \times 10^{20}$ eV. Since both of these features are signatures of protons, their observational confirmation means the indication that mass composition is dominated by protons. The shape of the dip allows admixture of nuclei not more than 10 - 15 %. The transition from galactic to extragalactic CRs is completed at $E_b \approx 1 \times 10^{18}$ eV. The appearance of galactic CRs at $E \leq E_b$ can be seen from behavior of modification factor in AGASA and HiRes experiments below E_b (see Fig. 3) and from flattening of calculated spectra for both rectilinear and diffusive propagation. The diffusive propagation makes flattening of the spectrum below E_b more pronounced [27, 28, 29]. One can see this spectrum behavior for the case of the Bohm diffusion in Fig. 6 (left panel, curve "extr. p"); the apparent falling-down shape of this curve is caused by multiplication of the spectrum by $E^{2.5}$. The intersection of this curve with the galactic spectrum, shown by dashed line, provides the transition from galactic to extragalactic CRs. The transition occurs at energy $E_{\rm tr} \approx 5 \times 10^{17}$ eV. The galactic component is found by subtracting the calculated extragalactic proton flux from the observed flux, given by the KASCADE and HiRes data. Since the energy of transition $E_{\rm tr}$ is close enough to the position of iron knee given by Eq. (2), the dip model fits perfectly the Standard Model of Galactic CRs. The galactic spectrum below the iron knee is presented by iron nuclei, and thus transition takes place sharply between iron nuclei and protons. The feature in the *observed spectrum*, which corresponds to the transition in the dip model is the *second knee* at energy $(4-8)\times10^{17}$ eV as observed in different experiments. The assumed generation spectrum in the dip model has $\gamma_g \approx 2.6 - 2.7$. Being extrapolated to $E_{\min} \sim 1$ GeV, such spectrum results in too high energy output of the sources. This problem is naturally solved with an assumption that the actual source spectrum has a standard shape with $\gamma_g = 2.0$ for non-relativistic shocks or $\gamma_g = 2.2 - 2.3$ for relativistic ones. However, the natural distribution of the sources over $E_{\max}$ [33] or luminosities [16] results in steepening of energy spectrum of generation rate $Q(E_g)$ per *unit volume* of the universe to larger γ_g, starting from some energy.

The prediction for elongation rate $X_{\max}(E)$ is shown in Fig. 7 (left panel). The characteristic feature of the dip model – sharp transition from galactic iron to extragalactic protons – results in steep increase of $X_{\max}(E)$ with E below 1×10^9 GeV in

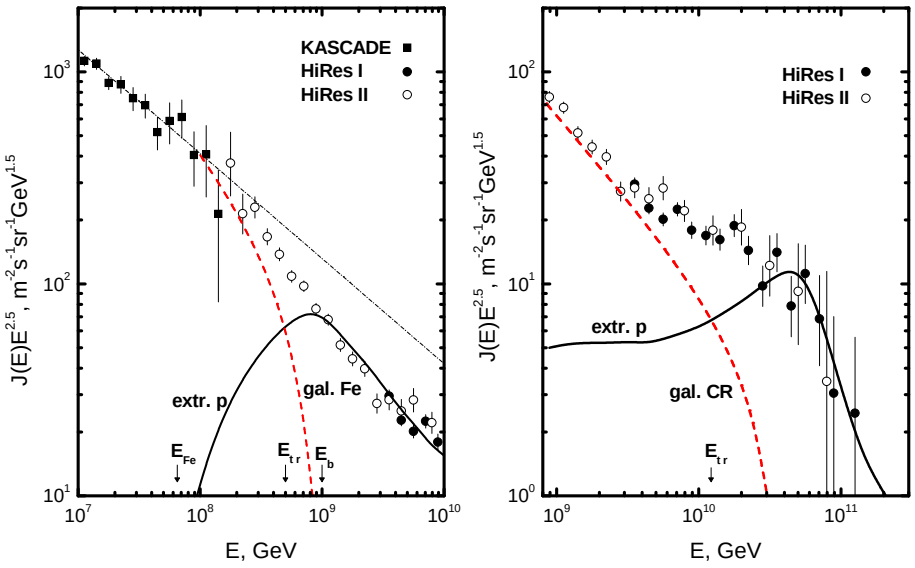

Fig. 6. Transition in the dip (left panel) and ankle (right panel) models. In both cases a solid line gives the calculated spectrum of extragalactic protons and a dashed line - spectrum of galactic iron. $E_{\rm tr}$ is the energy of intersection of galactic and extragalactic spectra and $E_{\rm Fe}$ gives the position of iron knee. $E_b = 1 \times 10^{18}$ eV in the left panel is the energy where transition from galactic to extragalactic CRs is completed.

contrast to the ankle model, where the increase of $X_{\rm max}(E)$ is less steep, because of very flat proton spectrum at $E \lesssim 1 \times 10^{18}$ eV. The observational data do not contradict the predicted steep increase of elongation rate below 1×10^{18} eV.

The left panel of Fig. 7 shows a reasonable agreement of the dip model with the bulk of experimental points in this figure, especially if one takes into account $20 - 25$ g/cm^2 of systematic error in all experiments. However, the detailed comparison of the dip prediction with the data of each experiment shows the different picture. While elongation rate predicted in the dip model agrees well with HiRes and HiRes-Mia data, it does not agree with the Auger data especially with two highest energy points.

The mixed composition model

The main concept of the mixed composition model (see Allard et al from [8], [9], [34], [35]) is based on the argument that any acceleration mechanism operating in the gas involves the different nuclei in acceleration process and thus the primary flux must have mixed composition. For injection into process of acceleration the authors assume A-dependent regime, instead of rigidity-dependent one (3) in the Standard Model, and obtain $J(E) \propto A^{\gamma_g - 1} E^{-\gamma_g}$ instead of Eq. (5) valid for the Standard Model. It results in higher abundance of CRs by heavy elements in comparison with the Standard Model. In fact, as discussed in [16], there are the reasonable regimes of injections when abundance of heavy nuclei is suppressed. The UHE extragalactic nuclei propagating through infra-red (IR) and CMB radiation are efficiently photo-disintegrated starting with energy $E \sim 1 \times 10^{19}$ eV, while protons survive and therefore GZK feature is present in the mixed-composition model. At energy below 1×10^{17} eV the authors consider the mixed-composition spectrum [34] which is proportional to injection spectrum in the Galaxy:

$$Q_i(E) = x_i A_i^{\gamma_g - 1} K E^{-\gamma_g}, \qquad (9)$$

where K is a normalization constant, i is a type of nuclei, x_i are free parameters, which describe the source chemical composition, and γ_g is a spectral index, chosen to fit the data, with preferable values between 2.1 - 2.3, motivated by acceleration at the

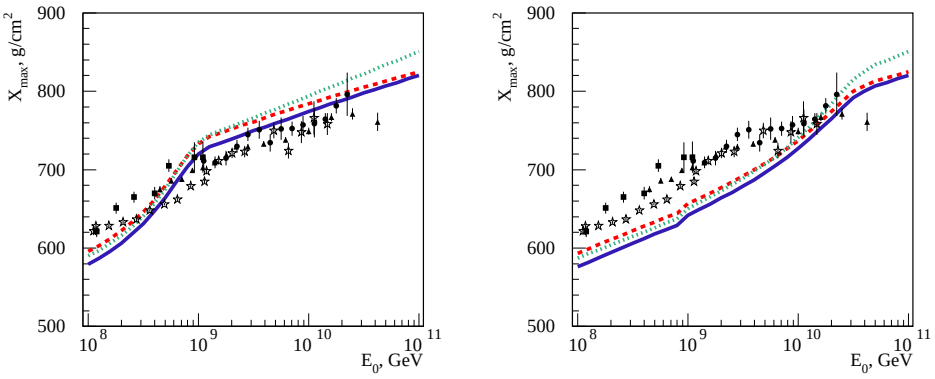

Fig. 7. Elongation rate for the dip model (left panel) and ankle model (right panel). The calculated elongation rates are shown by the solid lines for QGSJET [30] model of interaction, by dashed lines for QGSJET-II [31], and by dotted lines for SIBYLL [32]. The data points are measurements of Fly's Eye (stars), HiRes-Mia (squares), HiRes (circles) and Auger (triangles).

relativistic shocks. The cosmological evolution of the sources are included in calculations using factor $(1+z)^m$ up to $z_{\max}$ with different m, including $m = 0$, and different $z_{\max}$.

With (9) taken as generation spectrum, the authors calculate the diffuse spectrum at higher energies propagating protons and nuclei through IR and CMB radiation from the sources distributed uniformly in the universe. Using the calculated spectrum they fit the observed spectrum at energy higher than $E_a = 3\times10^{18}$ eV, which is thus the energy where the pure extragalactic spectrum starts, i.e. transition is completed.

The galactic component is found by subtraction of calculated extragalactic spectrum from the total observed spectrum. This procedure, adopted from [25], gives the spectrum below E_a as observed and provides the smooth transition to calculated extragalactic spectrum at E_a. Therefore, the part of the observed dip below E_a is reproduced in this procedure phenomenologically in contrast to the pair-production dip, which is accurately calculated.

The calculated spectrum and mass composition depends on parameters x_i in Eq. (9), γ_g, parameters of cosmological evolution m and $z_{\max}$, and therefore it is most flexible model among the three models at the discussion, which is able in particular to reproduce an arbitrary mass composition with some exception. The robust prediction for spectrum and mass composition is related to energy range $E > 1 \times 10^{19}$ eV, where the fraction of protons becomes large and steadily increasing, resulting thus in the GZK feature and almost pure proton composition, in contradiction with recent results of Auger.

The spectra and mass composition predicted in one of the versions of the mixed model [34] are displayed in Fig. 8. The mass composition is in a good agreement with the selected data of Fly's Eye (only stereo), HiRes (only stereo) and HiRes-Mia, shown in the figure. The predicted elongation rate has two break points, the first at $E_a = 3\times10^{18}$ eV, and the second at $E \approx 1 \times 10^{19}$ eV. The first one occurs when transition to extragalactic CRs is completed and evolution continues due to photodisintegration of nuclei, first iron, then CNO and finally helium. At energy $E \geq 1 \times 10^{19}$ eV (seen in the figure as $E = 1.3 \times 10^{19}$ eV) all nuclei are destroying faster and at $E \geq 3\times10^{19}$ eV the composition becomes strongly proton dominated with GZK feature in the energy spectrum.

The first break point agrees with the Auger feature in elongation rate, but prediction of increasing $X_{\max}$ at the second break point, i.e. at $E > 1 \times 10^{19}$ eV, contradicts to decreasing of $X_{\max}$ in the Auger data.

Discussion and Conclusions

The region of transition from galactic to extragalactic CRs at energy between $1 \times 10^{17} - 1 \times 10^{19}$ eV is the key energy range for understanding the origin of CRs. At low energy part it includes the high energy end of galactic CRs. The

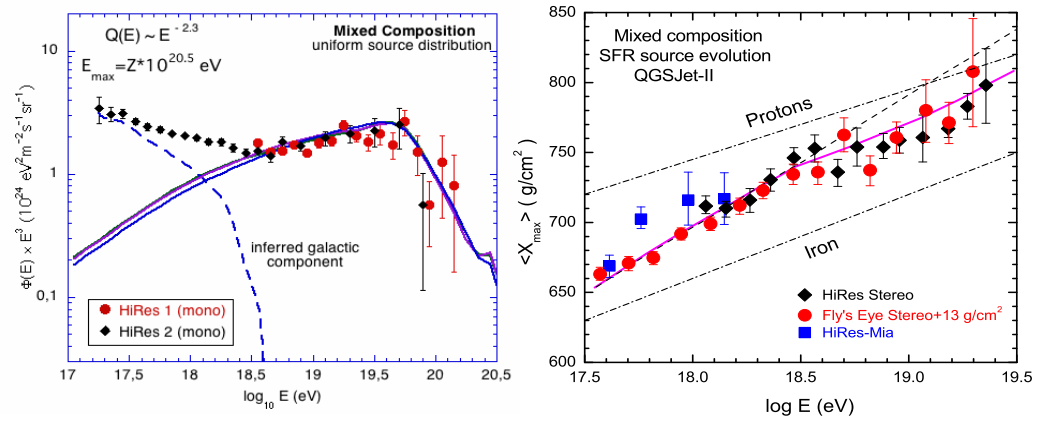

Fig. 8. The spectrum (left panel) and elongation rate (right panel) for the mixed model [34] with $\gamma_g = 2.3$, $E_a = 3\times10^{18}$ eV, cosmological source evolution $(1+z)^3$ at $z \leq 1.3$ and a set of parameters x_i (see the text). At $E > 3\times10^{19}$ eV the spectrum is strongly proton-dominated and is characterized by GZK cutoff (left panel). The mass composition evolves from almost pure iron composition at $E \approx 3\times10^{17}$ eV to the lighter composition due to enrichment by protons and light nuclei of extragalactic origin. At energy $E_a = 3\times10^{18}$ eV the transition to pure extragalactic component is completed and chemical composition evolution proceeds further due to photo-disintegration of the nuclei. At energy $E \approx 1.3\times10^{19}$ eV, seen in the plot, all nuclei are disappearing faster than before and composition becomes strongly proton-dominated at $E \geq 3\times10^{19}$ eV.

information on maximum energy of acceleration, chemical composition and propagation in Galaxy at these energies will clarify the total picture of origin at lower energies. The low energy part of UHECRs is important for understanding of origin of UHECRs and their propagation in extragalactic magnetic fields. The transition from galactic to extragalactic CRs is the central issue of this energy region.

There are two detectors which cover partially the above-mentioned region: KASCADE-GRANDE [36] and TALE [37]. There are also the proposals to extend the observations of Auger to energy $E \sim 1\times10^{17}$ eV (see e.g. [38]). The Auger detector has great potential to explore this region, building more dense part of the detector covered with fluorescent, scintillator and muon detectors.

The basic information which can be obtained includes precise measurement of energy spectra and mass composition (there is little hope to detect anisotropy in this energy region, though in some models the galactic sources can be observed in protons with energy $E \lesssim 10^{18}$ eV [25]).

At present we have the sufficiently good data on spectra and mass composition at energy range $1\times10^{18} - 4\times10^{19}$ eV. The spectra are measured with high statistics (especially in case of the Auger detector), but problem is the accuracy of energy determination. From quite disappointing Fig. 5 (left panel) one concludes that scales of energy determination is quite different in all detectors. Energy calibration with help of the pair-production dip suggests that energy measured by scintillator detectors is systematically higher than that by the fluorescence detectors and it gives a reasonable recipe of increasing energies given by fluorescent method and decreasing it for the scintillation method. In this case the curves 'Yakutsk' and 'Akeno-AGASA' in Fig. 5 go down and 'HiRes' and 'Auger' - up. For HiRes, AGASA and Yakutsk the method of calibration with help of dip works successfully (see Fig. 4) with energy shift within the allowed systematic errors, but for Auger it requires the shift by factor 2 greater than systematic error.

The pair-production proton dip in terms of modification factor is an excellent tool to measure *spectrum shape* independently of absolute flux. From Fig. 3 one sees the excellent agreement of the theoretical dip with data of AGASA, HiRes and Yakutsk. By the standards of cosmic-ray physics the agreement with Auger data is also good, but χ^2 for comparison with SD data is very large. This is a result of very big statistics in the surface detectors at lowest energies $E \geq 4.5\times10^{18}$ eV. In the lowest energy bin at $E = 4.5\times10^{18}$ eV

there are 4128 events and the error in determination of flux provided mostly by this statistics is $\delta J/J = 0.024$. The theoretical value of modification factor at this energy is only 14% higher than experimental value, but owing to very small $\delta J/J$, the contribution of this bin to χ^2 is 99.27 ! Most probably the other sources of errors should be included in the bins with small $\delta J/J$, and a possible source of this error is the energy errors which are changing randomly inside a bin. These could be statistical errors and energy-dependent part of systematic errors. Assuming that number of events are distributed in a bin as $N(E) = KE^{-\gamma}$ one obtains $\delta J/J = \gamma(\delta E/E)_r$, where $(\delta E/E)_r$ is the random energy error inside the bin. The estimated value $\delta J/J$ is much larger than what obtained in Auger analysis for all reasonable values of $(\delta E/E)_r$ and γ. More generally, according to Markus Roth's remark, χ^2 analysis is not adequate for the cases of small $\delta J/J$ and large $(\delta E/E)$. At this stage of analysis we do not consider Fig. 3 as contradiction with Auger data.

Coming to the transition from galactic to extragalactic CRs, we emphasize that at present there are only two experimental methods to study it: measuring the spectrum and mass composition. The transition will be clearly seen if spectrum of iron nuclei and that of protons are measured separately (see Fig. 6), but even without this ideal possibility the total spectrum has signatures of transition in the form of the spectral features - *second knee* in case of the dip model and *ankle* in case of the ankle model. The spectrum can be measured nowadays with high accuracy and its shape contains the information about mass composition, which is the other characteristic of the transition. The pair-production dip with its specific shape is a signature of proton-dominated composition (nuclei contribution should be not more than 10 -15 % [5]) and its observational confirmation is an argument not weaker than that due to $X_{\max}$ measurement (we remind that only two free parameters are involved in describing about 20 energy bins in each experiment).

The mass composition gives another way to test the transition. The best method at present is given by measuring of elongation rate $X_{\max}(E)$. Unfortunately this method has many uncertainties, including those in value of fluorescent yield, absorption of UV light in the atmosphere and uncertainties in the models of interactions, needed to convert the tested mass composition into $X_{\max}$. The systematic errors in measuring $X_{\max}$ can be as large 30 g/cm^2 to be compared with difference about 100 g/cm^2 between $X_{\max}$ for protons and iron. The better sensitivity for distinguishing different nuclei is given by distribution over $X_{\max}$ [26].

There are three models of the transition: ankle, dip and mixed-composition model. They differ most notably by the energy of transition (ankle: $E \sim 1 \times 10^{19}$ eV, dip: $E \approx 1 \times 10^{18}$ eV and mixed composition model $E \approx 3 \times 10^{18}$ eV), and by mass composition of extragalactic component (protons - for the ankle model, proton-dominated - for the dip model and mixed composition - for the third model).

The *ankle model* contradicts the Standard Model of Galactic CRs (energy where galactic flux is half of that observed is two orders of magnitude higher than energy of iron knee) and severely disagrees with $X_{\max}$ measured in all experiments at $(1.5 - 5) \times 10^{18}$ eV.

The *dip model* is based on well confirmed signature of proton interaction with CMB - pair-production dip. The two other models must assume that agreement of pair-production dip with data is accidental and the observed dip is produced by two components, galactic and extragalactic. The dip model assumes the iron-dominated galactic flux below 5×10^{17} eV and proton-dominated extragalactic flux above 1×10^{18} eV. This mass composition is confirmed by HiRes and HiRes-Mia data for elongation rate. It does not contradict the bulk of all data on $X_{\max}$, but contradicts $X_{\max}$ measured by Auger, especially the highest energy points. The generation spectrum in this model is E^{-2} or $E^{-2.2}$ as needed by shock acceleration with a steepening to $\gamma_g = 2.7$ due to distribution of sources over maximum energy of acceleration of source luminosities. The proton-dominated composition can be produced in some models of injection to the shock acceleration.

The *mixed composition model* assumes mixed composition generation spectrum for extragalactic component with generation index 2.1 - 2.3. It has many free parameters, most notably ones describing the mass composition of the genera-

tion spectrum, and thus it can in principle explain any observed mass composition. However, this model has a robust prediction at energy $E \gtrsim 3 \times 10^{19}$ eV: proton-dominated composition and the GZK feature. As far as Auger elongation rate is concerned, the mixed composition model explains well the break in elongation rate at 2×10^{18} eV and contradicts the two Auger points at $E > 2 \times 10^{19}$ eV. The energy where transition to extragalactic CRs is completed in most versions of this model equals $E \approx 3 \times 10^{18}$ eV. Much better quality of data on $X_{\max}$ is needed to distinguish the dip and mixed-composition models by $X_{\max}$ measurements. Probably it is possible to do using $X_{\max}$ distribution [26].

We will comment now on agreement of the transition models with the measured galactic spectrum. For all three models it is reached by the formal subtraction procedure: the galactic spectrum is found as difference between measured total spectrum and calculated extragalactic spectrum. But the galactic spectrum calculated in the Standard Model at $E \gtrsim 1 \times 10^{17}$ eV is very steep and, as was demonstrated in [39], for diffusive model of propagation all three models contradict the calculated galactic spectrum, the dip model to the less extent. Strictly speaking this contradiction is produced by exponential cutoff in the acceleration spectrum at $E > E_{\max}^{\rm acc}$.

The most consistent conclusions on nature of observed UHECRs are obtained at present by HiRes detector: it has confirmed the pair-production dip and thus proton-dominant composition at $1 \times 10^{18} - 4 \times 10^{19}$ eV, the $X_{\max}$ measurements agree with proton-dominant composition at $E > 1 \times 10^{18}$ eV , and $E_{1/2}$ measurement confirms that steepening of the spectrum observed at $E > 4 \times 10^{19}$ eV is really the GZK cutoff. Therefore, according to these data CRs observed at $E \gtrsim 1 \times 10^{18}$ eV are extragalactic protons exhibiting two signatures of interaction with CMB: pair-production dip and GZK feature.

Acknowledgments

I am grateful to Askhat Gazizov for the joint work on analysis of Auger data and for numerous discussions. I acknowledge the illuminating discussions about data errors with Markus Roth, Gianni Navarra and Karl-Heinz Kampert. My collaborators R. Aloisio, P. Blasi and S. Ostapchenko are thanked for joint work on related subject and for many discussions. This work is supported in part by *ASI* through grant *WP 1300* (theoretical study).

References

[1] K. Greisen, Phys. Rev. Lett. 16, (1966) 748; G. T. Zatsepin and V. A. Kuzmin, Pisma Zh. Experim. Theor. Phys. 4 (1966) 114.

[2] V. S. Berezinsky and S. I. Grigorieva, Astron. Astroph. 199 (1988) 1.

[3] T. Stanev et al, Phys.Rev. D 62 (200) 093005.

[4] V. Berezinsky, A. Z. Gazizov and S. I. Grigorieva, Phys. Rev. D 74 (2006) 043005.

[5] V. Berezinsky, A. Z. Gazizov and S. I. Grigorieva, Phys. Lett. B 612 (2005) 147.

[6] C. T. Hill and D. N. Schramm, Phys. Rev. D 31 (1985) 564.

[7] S. Yoshida and M. Teshima, Progr. Theor. Phys. 89 (1983) 833.

[8] A. M. Hillas, Nucl. Phys. Proc. Suppl. 136 (2004) 139; J. Phys. G 31 (2005) R95; astro-ph/0607109;
D. De Marco and T. Stanev, Phys. Rev. D 72 (2005) 081301;
D. Allard et al., Astron. Astrophys. 443 (2005) L29;
T. Wibig and A. W. Wolfendale, J. Phys. G 31 (2005) 255.

[9] D. Allard, E. Parizot, A. V. Olinto, Astropart. Phys. 27 (2007) 61.

[10] A. R. Bell and S. G. Lucek, MNRAS 321, (2001) 433; A. R. Bell, MNRAS 353, (2004) 550.

[11] E. Amato and P. Blasi, MNRAS 371 (2004) 1251; E. Amato and P. Blasi, MNRAS Lett. 364 (2005) 76.

[12] V. S. Ptuskin and V. N. Zirakashvili, Advances in Space Research, 37 (2006) 1898.

[13] D. Ellison, L. O. C. Drury, J.-P. Meyer, Astrophys. J. 487 (1997) 197.

[14] J.-P. Meyer, L. O. C. Drury, D. Ellison, Astrophys. J. 487 (1997) 182.

[15] E. G. Berezhko, L. T. Ksenofontov, J. Exp. Theor. Phys. 89 (1999) 391.

[16] R. Aloisio et al., Astropart. Phys. 27 (2007) 76.

[17] V. S, Berezinsky et al., *Astrophysics of Cosmic Rays* (North Holland, Amsterdam, 1990).

[18] D. De Marco, P. Blasi and T. Stanev, *Numerical propagation of high energy cosmic rays in the Galaxy I: technical issues*, arXiv:0705.1972v1[astro-ph].

[19] L. D. Landau and E. M. Lifshitz, *Electrodynamics of Continuous Media* (New York, Pergamon Press, 1987).

[20] E. G. Berezhko et al., Astron. Astroph. 410 (2003) 189.

[21] E. G. Berezhko and H. J. Völk, *Spectrum of cosmic rays, produced in supernova remnants*, arXiv:0704.1715v1[astro-ph].

[22] R. U. Abbasi et al. (HiRes Collaboration), Phys. Rev. Lett. 92 (2004) 151101; V. P. Egorova et al. (Yakutsk Collaboration), Nucl. Phys. B (Proc. Suppl.) 3 (2004) 136;K. Shinozaki et al. (AGASA Collaboration), Nucl. Phys. B (Proc. Suppl.) 3 (2006)151; M. Honda et al. (Akeno Collaboration), Phys. Rev. D 70 (2003) 525; D. J. Bird et al. (Fly's Eye Collaboration), Ap. J. 424 (1994) 491; M. Roth (Pierre Auger Collaboration), *Measurement of the UHECR energy spectrum using data from the Surface Detector of the Pierre Auger Observatory*, astro-ph/0706.2096;L. Perrone (Pierre Auger Collaboration), *Measurement of the UHECR energy spectrum from hybrid data of the Pierre Auger Observatory*, astro-ph/0706.2643.

[23] D. De Marco, P. Blasi, and A. V. Olinto, J. Cosm. Astrop. Phys. 01 (2006) 002.

[24] M. Teshima, Proceedings of 30th ICRC, Merida, Mexico, Vol. 6, p. 329.

[25] V. Berezinsky, S. Grigorieva and B. Hnatyk, Astrop. Phys. 22 (2004) 617.

[26] R. Aloisio et al., *Signatures of the transition from galactic to extragalactic cosmic rays*, astro-ph/0706.2834.

[27] M. Lemoine, Phys. Rev. D 71 (2005) 083007.

[28] R. Aloisio and V. Berezinsky, Astrophys. J. 625 (2005) 249.

[29] V. Berezinsky and A. Z. Gazizov, *Diffusion of Cosmic Rays in the Expanding Universe. II. Energy Spectra of Ultra-High Energy Cosmic Rays* , astro-ph/0702102.

[30] N. N. Kalmykov, S. S. Ostapchenko and A. I. Pavlov, Bull. Russ. Acad. Sci. Phys. 58 (1994) 1966; Nucl. Phys. Proc. Suppl. 52B (1997) 17.

[31] S. Ostapchenko, Phys. Rev. D 74 (2006) 014026; Nucl. Phys. Proc. Suppl. 151 B (2006) , 143.

[32] R. S. Fletcher et al., Phys. Rev. D 50 (1994) 5710.

[33] M. Kachelrieß and D. Semikoz, Phys. Lett. B 634 (2006) 143.

[34] D. Allard, A. V. Olinto and E. Parizot, *Signatures of the extragalactic cosmic-ray source composition from spectrum and shower depth measurements*, astro-ph/0703633.

[35] N. Globus, D. Allard and E. Parizot, *Propagation of high-energy cosmic rays in extragalactic turbulent magnetic fields: resulting energy spectrum and composition* , astro-ph/0709.1541.

[36] K.-H. Kampert (for KASCADE Grande collaboration) Nucl. Phys. B. (Proc. Suppl.) 122 C (2003) 422.

[37] D. R. Bergman (for TA/TALE Collaboration) Proceedings of 29th ICRC (Pune) v.8, 141 (2005); ibid C. C. H. Jui v.8, 101 (2005).

[38] M.C. Medina et al, *Enhancing the Pierre Auger Observatory to the* 10^{17} *to* $10^{18.5}$ *eV Range: Capabilities of an Infill Surface Array*, astro-ph/0607115.

[39] C. De Donato and G. A. Medina-Tanco, *The end of the Galactic spectrum*, arXiv:0708.0203v2[astro-ph].